Effects of the preheating temperature on flame-assisted spray pyrolysis of nickel-rich cathode materials

Effects of the Preheating Temperature on Flame-Assisted Spray Pyrolysis of Nickel-Rich Cathode Materials

Jianan Zhang[a], Valerie L. Muldoon[a], Sili Deng[a,*]

[a]*Department of Mechanical Engineering, Massachusetts Institute of Technology, Cambridge, USA*

Abstract

Reducing the cost and improving the performance of lithium-ion batteries (LIBs) are crucial for their applications in transportation electrification and grid energy storage. Much research effort has been devoted to develop novel synthesis methods for LIB cathodes, since traditional methods such as coprecipitation suffer long synthesis time and complex steps. In contrast, flame-based spray methods have great potential in manufacturing LIB cathode materials due to their features such as continuous, fast, and scalable operation. Nevertheless, flame-based spray methods also need improvement in controlling the morphology and improving the electrochemical performance of LIBs. The current work demonstrated a modified flame-assisted spray pyrolysis (FASP) method that used a preheating section for morphology control and electrochemical performance enhancement. The goal is to investigate the effect of preheating temperature on the particle morphology and electrochemical performance of $Li(Ni_{0.8}Co_{0.1}Mn_{0.1})O_2$ (NCM811) cathode materials. Results showed that the preheating temperature could significantly alter the particle morphology by affecting the drying process. X-ray diffraction measurements demonstrated that the cation mixing level of NCM811 samples was sensitive to the preheating temperature, where introducing the preheating section was effective in inhibiting cation mixing and improving cation ordering at certain temperatures. However, a preheating temperature higher than 325 °C would notably encourage cation mixing. Moreover, the electrochemical tests showed that increasing the preheating temperature could improve the discharge capacity and stabilize the long-time cycling performance. Overall, carefully choosing the preheating temperature of FASP not only improved the particle uniformity by inhibiting the formation of hard-to-break agglomerations in calcinated powders, but also enhanced the electrochemical performance by hindering cation mixing.

Keywords: Flame-assisted spray pyrolysis; nickel-rich cathode; preheating temperature; morphology; electrochemical performance

*Corresponding author.

1. Introduction

Lithium-ion batteries (LIBs) play an increasingly critical role in transportation electrification and grid energy storage of renewable energy such as wind and solar. Unfortunately, the cost of LIB is one of the main barriers limiting its large-scale application. Among different cost factors, cathode materials are an essential one because they are the main contributor that accounts for 39% of the material cost [1,2]. Currently, commonly used cathode materials are lithium iron phosphate ($LiFePO_4$), lithium-nickel-cobalt-aluminum oxide (NCA), and lithium-nickel-cobalt-manganese oxide (NCM). NCM is promising because of its potential in lowering cobalt and increasing nickel content for higher capacity and lower material cost. The most widely used methods for synthesizing NCM cathode materials are the solid-state and coprecipitation methods. Nevertheless, these methods encounter challenges in balancing the manufacturing cost and the material performance. For example, the coprecipitation method suffers issues of using non-continuous batch-based reactors, having many complex operation units, and being a slow synthesis process [3], resulting in a high manufacturing cost that contributes to 46% of the cathode material cost [4].

In contrast, spray-based methods are promising candidates to reduce the manufacturing cost due to having continuous flow conditions, a simple operation system, and a short synthesis time. As a result, spray-based methods have been employed for synthesizing a wide range of materials [5,6]. Among these methods, flame-related ones are preferred for large-scale production due to the high-temperature working condition that allows fast precursor decomposition and the potential for scaling up. For instance, flame spray pyrolysis is used for commercially producing TiO_2 and carbon black at the rate of tons per hour [6].

Different types of NCM cathode materials have been synthesized using flame-based synthesis methods. It was demonstrated that the flame-based spray method could integrate with *in situ* coating process. Abram et al. reported a flame aerosol synthesis method to produce $Li(Ni_{1/3}Co_{1/3}Mn_{1/3})O_2$ (NCM111) and $Li(Ni_{0.8}Co_{0.1}Mn_{0.1})O_2$ (NCM811) [7]. With the same method, Yan et al. demonstrated that NCM811 doped with dysprosium could notably improve the cycling performance and thermal-chemical stability [8]. Moreover, Zhang et al. used glycerol as fuel to synthesize NCM111 and $Li(Ni_{0.8}Co_{0.15}Al_{0.05})O_2$ (NCA) [9,10]. They found that the high-temperature flame played an important role in ensuring less porous particles and a shortened post-annealing time. Therefore, flame-based methods are capable of producing cathode material with desired performance. Moreover, a techno-economic analysis has confirmed the potential of using flame-assisted spray pyrolysis to reduce the manufacturing cost of cathode materials [11].

Although flame-based spray methods have various advantages over other methods, especially due to their potential in reducing the manufacturing cost, current flame-based spray methods still face challenges in matching the electrochemical performance to commercial methods such as coprecipitation. Therefore, different strategies have been applied to investigate the operating parameters such as the solution concentration [12], solvent type [9], operating temperature [7,12], dopants [8], post-calcination conditions [13], and atomization method [3] on the performance of the synthesized cathode materials. For flame-based methods, the droplet drying and pyrolysis process is considered critical in achieving desired particle morphology and electrochemical performance.

A simple and useful strategy to control the drying and pyrolysis process is introducing a preheating section prior to the high-temperature flame in the synthesis setup. This strategy can be adapted for a flame-assisted spray pyrolysis method (FASP). The preheating temperature was found to prompt homogeneous precipitation prior to the flame and produce more uniform materials [7]. Moreover, combining the preheating section with flame produced denser particles than the sample using only low-temperature drying [10]. Unfortunately, there are no comprehensive studies examining the role of preheating in FASP in detail. Therefore, the current work investigated the effect of preheating temperature on the particle morphology and electrochemical performance of nickel-rich NCM811 that is considered as the state-of-the-art cathode material. The provided information would be useful for paving the way for producing high-performance NCM811 cathode materials with a low-cost route, which is meaningful for large-scale applications.

2. Experimental

2.1 Material synthesis

The schematic of the synthesis process is demonstrated in Figure 1. First, the precursor solution was prepared by dissolving lithium nitrate ($LiNO_3$), nickel nitrate hexahydrate ($Ni(NO_3)_2{\cdot}6H_2O$), manganese nitrate tetrahydrate ($Mn(NO_3)_2{\cdot}4H_2O$), and cobalt nitrate hexahydrate ($Co(NO_3)_2{\cdot}6H_2O$) in deionized water with a concentration of 2 mol/L. 10% excess lithium nitrate was added to compensate the Li loss during the synthesis process, so the molar ratio of Li:Ni:Mn:Co is 1.1:0.8:0.1:0.1 in the prepared solution.

The solution was fed to a 1.7 MHz homemade ultrasonic nebulizer to generate droplets. Air was used as carrier gas (5 L/min) to carry droplets to a preheating tube (1.5 m in length, 47.5 mm in inner diameter). The preheating temperature (T_p) was defined as the tube wall temperature, which was changed in the range of 25 °C (room temperature) to 375 °C with a step of 50 °C. The way of defining the

preheating temperature follows the commonly used method in different spray-based synthesis routes for cathode material synthesis [3,12].

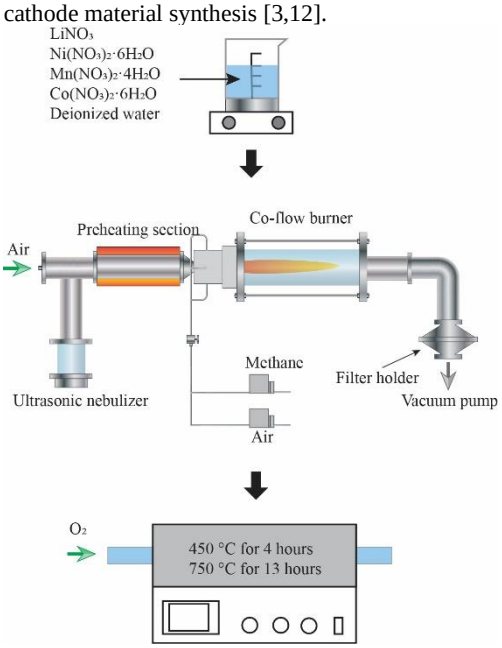

Fig. 1. Schematic of NCM811 synthesis process.

Then, the droplets/particles entered a premixed co-flow burner for further decomposition. The burner used a methane/air mixture at a constant equivalence ratio of 0.65 and a flow rate of 16 L/min. After passing through the flame, solid particles were generated and collected by a filter. The as-synthesized powder was then calcinated in a tube furnace at 450 °C for 4 hours and then 750 °C for 13 hours with an oxygen flow of 0.25 L/min.

2.2 Characterization methods

A PANalytical X'Pert PRO X-ray diffractometer using monochromatic, nickel filtered Cu Kα radiation (Kα1 = 1.540598 Å and Kα2 = 1.544426 Å) was used for X-ray diffraction (XRD) tests. The XRD was performed in the 2θ range of 10 - 90° with a step size of 0.01° s^{-1}. A Zeiss Merlin high-resolution scanning electron microscope was utilized to perform scanning electron microscopy (SEM). FEI Tecnai (G2 Spirit TWIN, 120 kV) was used to conduct transmission electron microscope (TEM) imaging. Agilent ICP-OES 5100 VDV was employed to perform inductively coupled plasma-optical emission spectrometer (ICP-OES) testing to measure the ratio of elements in samples.

2.3 Electrochemical test

The calcinated sample was then tested for its electrochemical performance by using CR2032-type half-cells. First, the cathode electrode was prepared as a slurry by mixing NCM811 powder as the active material, polyvinylidene fluoride (PVDF) as the binder, and carbon black as the conductive additive at a weight ratio of 8:1:1. The slurry was then coated on an aluminum film (15 μm) with an active material loading of 2.8±0.2 mg/cm^2. The aluminum film was then vacuum dried in an oven at 100 °C for 24 hours. Then, cathode electrode disks were cut and pressed at a pressure of 7 MPa. Coin cells were then assembled in an argon-filled glovebox with controlled oxygen and moisture level (O_2 < 1 ppm, H_2O < 1 ppm). Besides the prepared cathode electrode, the coin cell used a Li metal disk as the anode, a separator (Celgard 2320), and a commercial electrolyte with 1 M $LiPF_6$ in ethylene carbonate (EC) and diethyl carbonate (DEC) (EC:DEC = 1:1 v/v). The galvanostatic charge-discharge study was performed using a Land CT3001A battery tester in the potential range of 2.7 – 4.3 V at different C-rates (1C = 200 mA/g).

3. Results and Discussion

The as-synthesized and calcinated FASP samples were first examined for their morphology. Significant morphology differences are noticed in Fig. 2 when the preheating temperature changes. At the room temperature of 25 °C without preheating, irregularly-shaped particles are present in the as-synthesized sample shown in Fig. 2(a). The particles are apparently broken pieces of hollow particles with a shell. As a result, the calcinated powder comprises agglomerated nanoscale irregularly-shaped primary particles. Similar phenomena are observed for samples with preheating temperatures of T_p at 75 °C (Fig. 2(b)) and 125 °C (Fig. 2(c)). Particularly, particles with a hollow structure can be noticed clearly in Fig. 2(c). Then, spherical particles start to appear in the as-synthesized sample of T_p of 175 °C (Fig. 2(d)). The calcinated sample of T_p at 175 °C also contains easily identified spherical particles. As T_p increases to 225 °C (Fig. 2(e)), the spherical shape is maintained. However, a further increase of T_p to 275 °C leads to particles with holes on the surface as indicated in Fig. 2(f). Due to the small size of the hole, the calcinated sample in Fig. 2(f) has no apparent porous structure because of the crystal growth. As T_p is raised to 325 °C and 375 °C, particles with a concave shell dominate (Fig. 2(g) and (h)). As a result, the calcinated particles also have holes on the surface.

The evolution of the particle morphology with the change of T_p is the result of the change in the drying process. The mechanism is discussed schematically in Fig. 2(i). With no preheating or when the preheating temperature is low, the droplet is still in the liquid phase when passing the flame. Due to the high temperature of the flame, evaporation is fast. As a result, metal salts precipitate quickly on the droplet surface and form a shell [14]. Nevertheless, part of the solvent is still left inside the shell because of the fast shell formation. As the remaining solvent evaporates as vapor and builds up pressure inside the shell, it eventually breaks the shell and generates the

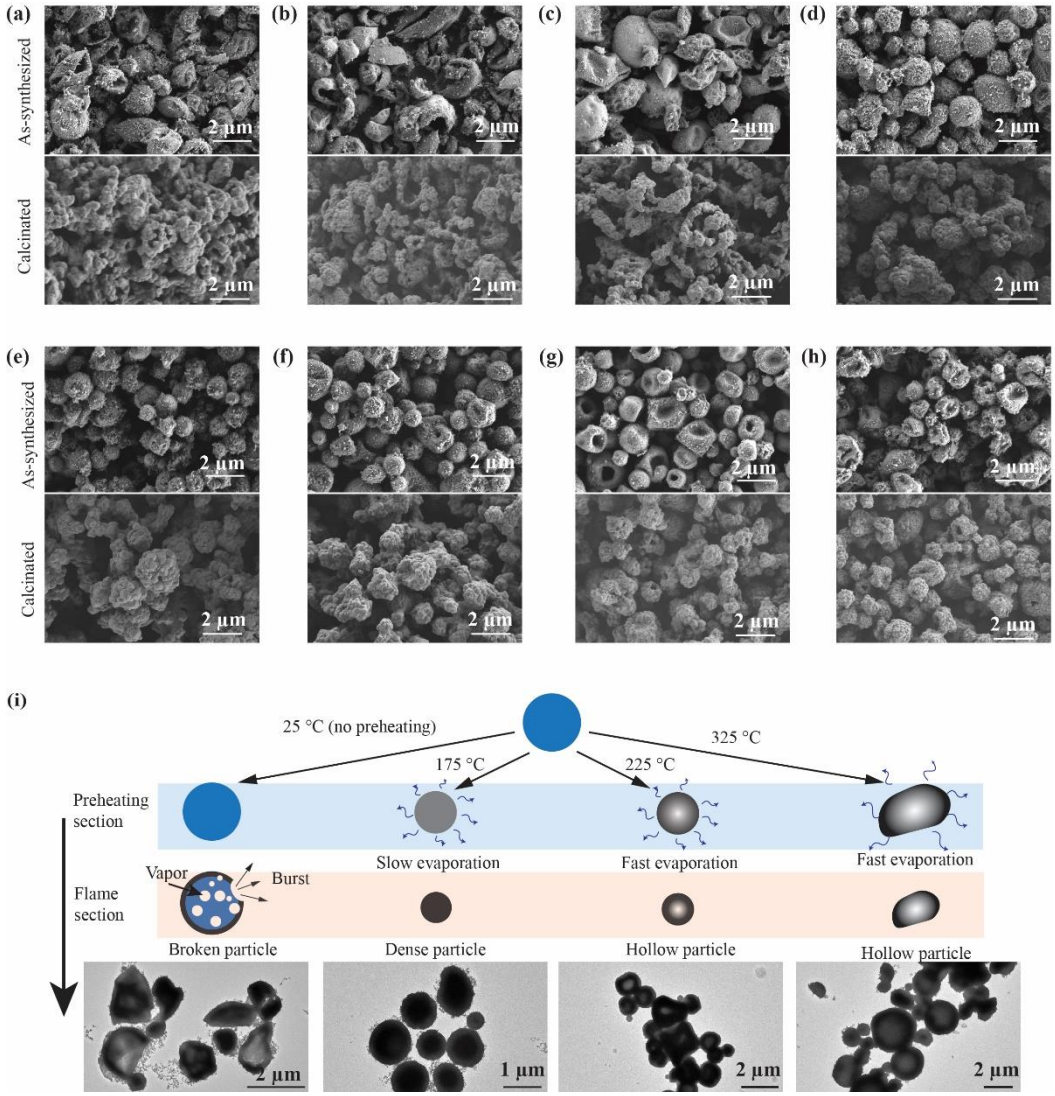

Fig. 2. SEM images of as-synthesized (top in each subplot) and calcinated (bottom in each subplot) samples with the preheating temperature of (a) 25 °C, (b) 75 °C, (c) 125 °C, (d) 175 °C, (e) 225 °C, (f) 275 °C, (g) 325 °C, (h) 375 °C, and (i) the proposed mechanism for the effect of preheating temperature on the particle morphology indicated by TEM images.

morphology shown in Fig. 2(a-c) [15]. When the preheating temperature is sufficiently high, early-stage evaporation at a relatively slow rate will tend to produce a particle with a dense structure as shown by the TEM image in Fig. 2(i) for the sample with T_p of 175 °C. Under this condition, passing through the flame is less likely to create broken particles due to largely removed solvent. As a result, the spherical shape dominates in Fig. 2(d) and (e). Nevertheless, the case at T_p of 225 °C starts to form a hollow structure that is indicated by the TEM image in Fig. 2(i). A further increase in the preheating temperature will cause fast precipitation and shell formation again. Nevertheless, as the preheating temperature (≤ 375 °C) is far less than the temperature near the flame (~ 900 °C), the solvent evaporation is slow so particles only have a collapsed surface but are not broken into pieces. In summary, changing the preheating temperature has largely changed the drying process so it is an efficient way to alter the particle morphology, adding an additional control parameter for designing particles with desired morphology. Generally speaking, samples with irregular shapes, especially broken shells, are less preferred for cathode material applications due to difficulties in controlling the size uniformity for ensuring consistency.

The elemental ratios of as-synthesized and calcinated samples are listed in Table S1. All samples have elemental molar ratios close to the chemical formula of NCM811 with the molar ratio of

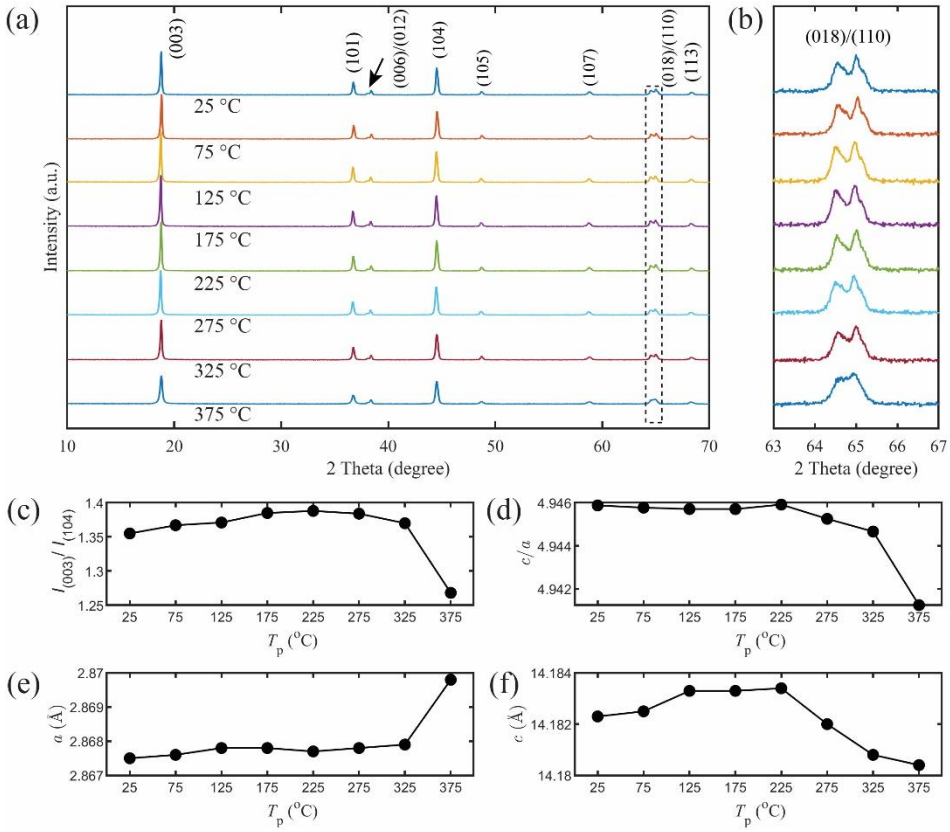

Fig. 3. (a) XRD patterns of calcinated samples with different preheating temperatures, (b) enlarged XRP patterns showing the peak pair of (018)/(110), (c) the ratio of lattice parameter *c*/*a*, (d) the ratio of the intensity of peak (103) to (104), (e) the change of lattice parameter *a* with T_p, and (f) the change of lattice parameter *c* with T_p.

Li:Ni:Co:Mn = 1:0.8:0.1:0.1, confirming the accurate control of the material composition with the current method. However, there is no clear trend about how the preheating temperature affects the composition of as-synthesized and calcinated samples.

The calcinated samples were examined further with XRD to demonstrate the crystal structure of samples with different preheating temperatures. XRD patterns in Fig. 3(a) confirm all annealed samples have clear diffraction peaks. They belong to the hexagonal α-$NaFeO_2$ type, defining a layered structure with an *R3m* space group without impurity phases [10]. Fig. 3(a) shows the enlarged diffraction peak pair of (018)/(110). As split (018)/(110) indicates an ordered layered structure [16], the sample at T_p of 375 °C has non-split peaks so it has a less ordered layered structure than others. The structure parameters were calculated based on the Rietveld refinement results and are available in Table S2. One important feature of nickel-rich cathode materials is the cation mixing, which is a result of the similar ionic radius of Ni^{2+} (0.69 Å) and Li^+ (0.76 Å) [17] because both Ni^{2+} and Li^+ have a coordination number of VI [18]. The level of cation mixing can be evaluated by the intensity ratio of peak (003) to (104), marked as $I_{(003)}/I_{(104)}$. Generally, a higher value of $I_{(003)}/I_{(104)}$ indicates a lower level of cation mixing. Moreover, the ratio of lattice parameter *c* to *a* (*c*/*a*) is an indicator of cation ordering. A larger *c*/*a* means a better cation ordering that is preferred for a well-defined hexagonal layered structure [19]. The layered structure is also confirmed by high resolution TEM images shown in Fig. S3.

As shown in Fig. 3(c), the value of $I_{(003)}/I_{(104)}$ first increases with increasing preheating temperature and then drops when the temperature increases further. Among them, the case with a T_p of 375 °C has the highest level of cation mixing. Fig. 3(d) shows that the value of *c*/*a* keeps almost constant up to 225 °C, then drops slightly when T_p increases further to 375 °C, indicating worsened cation ordering in samples with high preheating temperatures. Moreover, the trend of *c*/*a* evolution can be interpreted by the change of the lattice parameter *a* and *c*. As shown in Fig. 3(e), the value of *a* tends to increase slightly with the rising temperature. On the other hand, the value of *c* increases with the temperature first and then drops. For T_p from room temperature to 225 °C, both *a* and *c* change very mildly, so there are no obvious changes in the value of *c*/*a*. Nevertheless, as the preheating temperature increases above 225 °C, the lattice parameter *a* keeps increasing, whereas *c* starts to drop,

leading to a decreasing trend of *c*/*a*. The increased lattice parameter *a* and decreased lattice parameter *c* are both indicators of the reduced occupancy of Ni ion in 3a site [17]. These results imply that a high preheating temperature could facilitate cation disordering and cation mixing, so it is undesired for synthesizing NCM811.

Next, the electrochemical performance of samples using different preheating temperatures was examined. The first cycle discharge capacity and Coulombic efficiency at 0.1C are shown in Fig. 4(a) and (b), respectively. The selected charge-discharge curves of different samples are available in Fig. S1. Fig. 4(a) shows that the first cycle discharge capacity rises first from around 180 mAh/g to approximately 200 mAh/g and then decreases as the preheating temperature increases more. However, the Coulombic efficiency shows minor changes at around 85% until the preheating temperature reaches 325 °C but then drops when T_p reaches 375 °C. This could be the result of the high level of cation mixing and worsened cation ordering noticed for T_p at 375 °C in the XRD results.

Although the general trend of the discharge

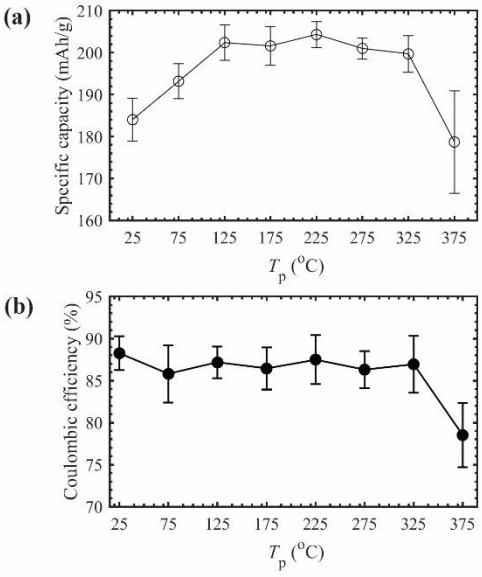

Fig. 4. (a) The first cycle discharge capacity and (b) the Coulombic efficiency at 0.1C in the potential range of 2.7 – 4.3V.

capacity matches the trend of the XRD, exceptions are cases with T_p = 25 °C and T_p = 75 °C. Both cases have relatively low values of discharge capacity even though ordered layered structure and low-level cation mixing were detected (Fig. 3), so the quality of crystallization is less likely to be the main reason for the low discharge capacity of samples with low preheating temperatures. Nevertheless, uneven films were noticed for cases with T_p = 25 °C and T_p = 75 °C when coating the slurry on the aluminum foil, one of them is shown in Fig. 5(a). The low-quality film could reduce the homogeneity of the electrical field, worsening the electrochemical performance [20]. To find the reason for uneven films, calcinated samples were ball-milled and examined for powder uniformity. Selected results are shown in Fig. 5 to represent as-synthesized samples with broken particles (T_p = 25 °C, Fig. 5(a)), solid spherical particles (T_p = 175 °C, Fig. 5(b)), and hollow particles (T_p = 375 °C, Fig. 5(c)). As the arrows in Fig. 5(a) show, agglomerated particles are present in the case with T_p of 25 °C, whereas cases with higher T_p of 175 °C and 375 °C have no obvious agglomerations. This confirms that the hard-to-break agglomerations formed in low T_p cases are responsible for the uneven film and the low discharge capacity. Moreover, this demonstrates that introducing the preheating section with properly controlled temperature can significantly improve the powder uniformity by inhibiting the formation of hard-to-break agglomerations.

Further comparisons were made in the cycling performance at the current rate of 1C. For the discharge capacity illustrated in Fig. 6(b), similar to the trend of discharge capacity at 0.1C, it increases first from 170 mAh/g (T_p = 25 °C) to a max value of 189 mAh/g (T_p = 225 °C) and then drops at higher temperatures (T_p > 225 °C). Moreover, Fig. 6(c) demonstrates that samples with T_p < 225 °C have lower retention ratios than those with a higher T_p. Different from the changing trend of the discharge capacity, the retention ratio remains high even when the preheating temperature increases to 375 °C, in spite of the low discharge capacity. The overall trend

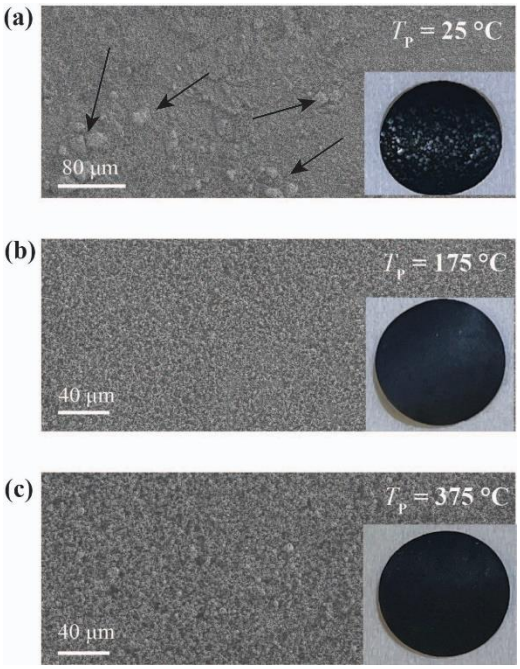

Fig. 5. SEM images and photos of prepared electrodes of milled samples after calcination (a) T_p = 25 °C, (b) T_p = 175 °C, and (c) T_p = 375 °C.

is shown by the cycling curves in Fig. 6(a), indicating

neither too low (< 125 °C) nor too high (> 325 °C) preheating temperatures are preferred for synthesizing NCM811 with high capacity and retention ratio.

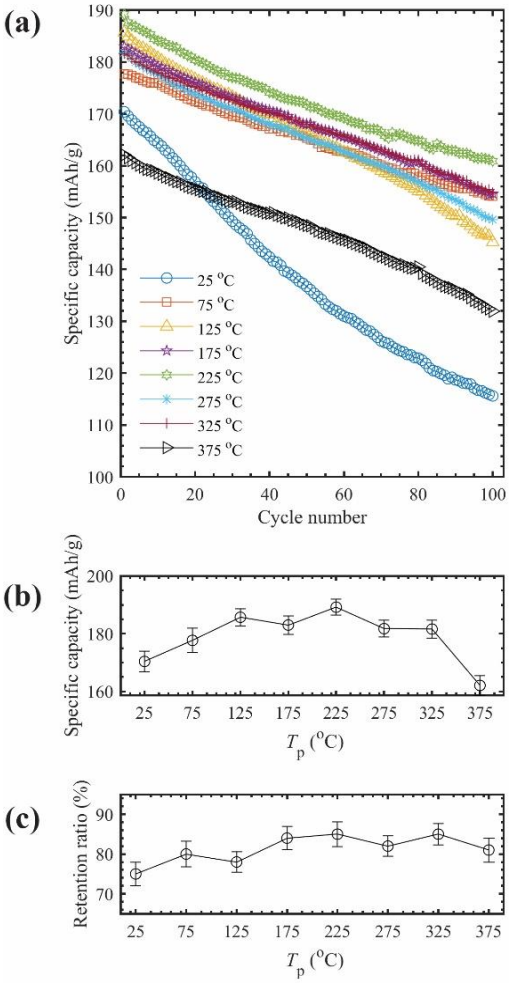

Fig. 6. (a) Cycling curves of different samples at 1C, (b) the discharge capacity of the 1st cycle at 1C, and (c) the retention ratio after 100 cycles.

The rate performance of different samples is shown in Fig. 7. For each sample, the assembled coin cell was cycled at different C-rates (5 times at each C-rate) in the order of 0.1C, 0.2C, 0.5C, 1C, 2C, 5C, and then back to 0.1C. Overall, the specific capacity decreases with the increasing C-rate because of the limitation of Li^+ diffusivity [21]. Fig. 7(a) shows that samples at T_p of 25 °C and T_p of 375 °C have lower capacities than other cases. The discharge capacity of the first cycle at different rates was then extracted and shown in Fig. 7(b). Consistent with the previous trend of the discharge capacity at 0.1C and 1C, the discharge capacity at lower C-rates (< 2C) increases and then declines with increasing preheating temperature. Nevertheless, a different trend was noticed when the C-rate increased. The capacity curve at 5C shows a concave shape in the temperature range of 125 °C to 325 °C, implying slightly worsened performance at high C-rates at medium temperatures around 225 °C.

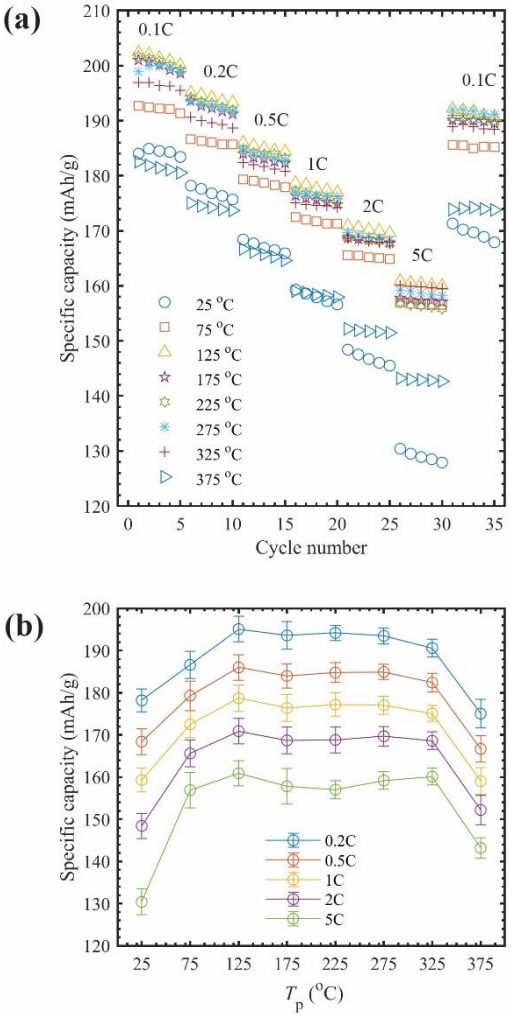

Fig. 7. (a) the rate performance of different samples and (b) the discharge capacity of the 1st cycle at different rates.

The difference could be related to the difference in particle morphology. It has been demonstrated in Fig. 2 that the particle is more porous at a low level of preheating temperature (< 125 °C) that results in broken particles and at a high level of preheating temperature (> 275 °C) that generates large hollow particles. Previous studies have demonstrated that the high C-rate performance would be improved when the particle has a more porous structure because of improved Li-ion diffusion [22,23].

Generally speaking, when the preheating temperature is well controlled, the morphology and electrochemical performance can be tuned accordingly. When the preheating temperature is too low, irregular particles were produced and caused hard-to-break agglomerations after heat treatment. The agglomerations are undesired for electrode

preparation and consequently worsen the electrochemical performance. In contrast, excessively high preheating temperatures tend to produce samples that suffer from a worsened layered structure and a high level of cation mixing. As a result, the sample synthesized at the high temperature of 375 °C has declined electrochemical performance. On the other hand, the preheating temperatures in the range of 175 °C to 325 °C can ensure well dispersed particle with ordered layered structure and a low level of cation mixing, which are desired for high-performance NCM811. Our current samples are comparable to those already reported [13,21], confirming that FASP can be used to produce high-quality cathode materials with simple modifications to the process.

4. Conclusion

The current work investigated the effect of the preheating temperature on the synthesized NCM811 cathode materials using flame-assisted spray pyrolysis. Results showed that the preheating temperature significantly impacted the morphology and electrochemical performance of the synthesized NCM811 cathode materials. Increasing the preheating temperature first eliminated the irregular particles and produced particles with spherical shapes. The temperature rise also improved the uniformity of calcinated powder by eliminating hard-to-break agglomerations. XRD results showed that the cation mixing level and cation ordering were also affected by the preheating temperature. The preheating temperatures below 325 °C led to a low-level cation mixing and ordered layered structure, whereas a high preheating temperature of 375 °C notably worsened the layered crystal structure. The electrochemical performance demonstrated that the discharge capacity at different C-rates (< 2C) increased first with the increasing preheating temperature and reached a stable performance in the range of 125 °C to 325 °C but then declined rapidly when the temperature rose to 375 °C. However, the Coulombic efficiency and retention ratio did not follow the same trend. Moreover, the capacity at a high rate of 5C shows that particles with a porous structure could enhance the performance. Therefore, different effects of the preheating temperature on the electrochemical performance should be balanced for practical applications. Overall, the current work demonstrated that the combustion-based spray method with simple modifications has the capability to produce high-performance nickel-rich cathode materials. Moreover, future works are recommended on tuning flame characteristics together with the preheating modification, which would further optimize the particle morphology and electrochemical performance.

Acknowledgements

The authors thank Yimeng Huang and Prof. Ju Li from the Department of Nuclear Science and Engineering, MIT, for their support in battery fabrication and testing.

Supplementary material

Supplementary material is provided.

References

[1] Turcheniuk K, Bondarev D, Amatucci GG, Yushin G. Battery materials for low-cost electric transportation. Mater Today (2020).

[2] Manthiram A. A reflection on lithium-ion battery cathode chemistry. Nat Commun (2020);11:1550.

[3] Oljaca M, Blizanac B, Du Pasquier A, Sun Y, Bontchev R, Suszko A, Wall R, Koehlert K. Novel Li(Ni1/3Co1/3Mn1/3)O2 cathode morphologies for high power Li-ion batteries. J Power Sources (2014);248:729–38.

[4] Wood DL, Li J, Daniel C. Prospects for reducing the processing cost of lithium ion batteries. J Power Sources (2015);275:234–42.

[5] Leng J, Wang Z, Wang J, Wu H-H, Yan G, Li X, Guo H, Liu Y, Zhang Q, Guo Z. Advances in nanostructures fabricated via spray pyrolysis and their applications in energy storage and conversion. Chem Soc Rev (2019);48:3015–72.

[6] Li S, Ren Y, Biswas P, Tse SD. Flame aerosol synthesis of nanostructured materials and functional devices: Processing, modeling, and diagnostics. Prog Energy Combust Sci (2016);55:1–59.

[7] Abram C, Shan J, Yang X, Yan C, Steingart D, Ju Y. Flame Aerosol Synthesis and Electrochemical Characterization of Ni-Rich Layered Cathode Materials for Li-Ion Batteries. ACS Appl Energy Mater (2019);2:1319–29.

[8] Yan C, Yang X, Zhao H, Zhong H, Ma G, Qi Y, Koel BE, Ju Y. Controlled Dy-doping to nickel-rich cathode materials in high temperature aerosol synthesis. Proc Combust Inst (2021);38:6623–30.

[9] Zhang J, Singh G, Xu S, Hamad K, Ratner A, Xing Y. A scalable approach of using biomass derived glycerol to synthesize cathode materials for lithium-ion batteries. J Clean Prod (2020);271:122518.

[10] Zhang J, Xu S, Hamad KI, Jasim AM, Xing Y. High retention rate NCA cathode powders from spray drying and flame assisted spray pyrolysis using glycerol as the solvent. Powder Technol

(2020);363:1–6.

[11] Zang G, Zhang J, Xu S, Xing Y. Techno-economic analysis of cathode material production using flame-assisted spray pyrolysis. Energy (2021);218:119504.

[12] Lengyel M, Atlas G, Elhassid D, Luo PY, Zhang X, Belharouak I, Axelbaum RL. Effects of synthesis conditions on the physical and electrochemical properties of Li1.2Mn0.54Ni0.13Co0.13O2 prepared by spray pyrolysis. J Power Sources (2014);262:286–96.

[13] Liang Y, Ku K, Lin Y, Yu L, Wen J, Lee E, Libera J, Lu J. Process Engineering to Increase the Layered Phase Concentration in the Immediate Products of Flame Spray Pyrolysis. ACS Appl Mater Interfaces (2021);13:26915–23.

[14] Eslamian M, Ashgriz N. Effect of Atomization Method on the Morphology of Spray-Generated Particles. J Eng Mater Technol (2006);129:130–42.

[15] Gurav A, Kodas T, Pluym T, Xiong Y. Aerosol Processing of Materials. Aerosol Sci Technol (1993);19:411–52.

[16] Weber R, Li H, Chen W, Kim C-Y, Plucknett K, Dahn JR. In Situ XRD Studies During Synthesis of Single-Crystal LiNiO2, LiNi0.975Mg0.025O2, and LiNi0.95Al0.05O2 Cathode Materials. J Electrochem Soc (2020);167:100501.

[17] Zhu J, Chen G. Single-crystal based studies for correlating the properties and high-voltage performance of Li[NixMnyCo1−x−y]O2 cathodes. J Mater Chem A (2019);7:5463–74.

[18] Shannon R. Revised effective ionic radii and systematic studies of interatomic distances in halides and chalcogenides. Acta Crystallogr Sect A (1976);32:751–67.

[19] Huang Z-D, Liu X-M, Oh S-W, Zhang B, Ma P-C, Kim J-K. Microscopically porous, interconnected single crystal LiNi1/3Co1/3Mn1/3O2 cathode material for Lithium ion batteries. J Mater Chem (2011);21:10777–84.

[20] Mohanty D, Hockaday E, Li J, Hensley DK, Daniel C, Wood DL. Effect of electrode manufacturing defects on electrochemical performance of lithium-ion batteries: Cognizance of the battery failure sources. J Power Sources (2016);312:70–9.

[21] Kim J, Lee H, Cha H, Yoon M, Park M, Cho J. Prospect and Reality of Ni-Rich Cathode for Commercialization. Adv Energy Mater (2018);8:1702028.

[22] Müller M, Schneider L, Bohn N, Binder JR, Bauer W. Effect of Nanostructured and Open-Porous Particle Morphology on Electrode Processing and Electrochemical Performance of Li-Ion Batteries. ACS Appl Energy Mater (2021);4:1993–2003.

[23] Chen Z, Wang J, Chao D, Baikie T, Bai L, Chen S, Zhao Y, Sum TC, Lin J, Shen Z. Hierarchical Porous LiNi1/3Co1/3Mn1/3O2 Nano-/Micro Spherical Cathode Material: Minimized Cation Mixing and Improved Li+ Mobility for Enhanced Electrochemical Performance. Sci Rep (2016);6:25771.